

ORCA - Online Research @ Cardiff

This is an Open Access document downloaded from ORCA, Cardiff University's institutional repository:https://orca.cardiff.ac.uk/id/eprint/109773/

This is the author's version of a work that was submitted to / accepted for publication.

Citation for final published version:

Coxall, Helen K., Huck, Claire E., Huber, Matthew, Lear, Caroline H., Legarda-Lisarri, Alba, O'Regan, Matt, Sliwinska, Kasia K., van de Flierdt, Tina, de Boer, Agatha M., Zachos, James C. and Backman, Jan 2018. Export of nutrient rich Northern Component Water preceded early Oligocene Antarctic glaciation. Nature Geoscience 11, pp. 190-196. 10.1038/s41561-018-0069-9

Publishers page: http://dx.doi.org/10.1038/s41561-018-0069-9

Please note:

Changes made as a result of publishing processes such as copy-editing, formatting and page numbers may not be reflected in this version. For the definitive version of this publication, please refer to the published source. You are advised to consult the publisher's version if you wish to cite this paper.

This version is being made available in accordance with publisher policies. See http://orca.cf.ac.uk/policies.html for usage policies. Copyright and moral rights for publications made available in ORCA are retained by the copyright holders.



Export of nutrient rich Northern Component Water preceded early Oligocene Antarctic glaciation

3

Authors: Helen K. Coxall¹, Claire Huck^{2,3}, Matthew Huber^{4,5}, Caroline H. Lear⁶, Alba Legarda-

- Lisarri¹⁰, Matt O'Regan¹, Kasia K. Sliwinska^{7,8}, Tina van de Flierdt², Agatha M. de Boer¹, James
 C. Zachos⁹ & Jan Backman¹
- 7

8 Affiliations:

- 9 ¹Department of Geological Sciences, Stockholm University, SE-106 91 Stockholm, Sweden.
- ²Department of Earth Science and Engineering, Imperial College London, South Kensington
 Campus, London SW7 2AZ, UK.
- ³Ocean and Earth Science, National Oceanography Centre Southampton, University of
- 13 Southampton, European Way, Southampton SO14 3ZH, UK.
- ⁴Department of Earth Sciences, University of New Hampshire, Durham, NH 03824, USA.
- ⁵Earth Systems Research Center, Institute for Earth, Ocean and Space Sciences, The University
 of New Hampshire, Durham NH, USA.
- ¹⁷⁶School of Earth and Ocean Sciences, Cardiff University, Main Building, Park Place, Cardiff
- 18 CF10 3AT, UK.
- ⁷Geological Survey of Denmark and Greenland, GEUS, Øster Voldgade 10, DK-1350,
- 20 Copenhagen K, Denmark.
- ⁸NIOZ Royal Netherlands Institute for Sea Research, Department of Marine Organic
- 22 Biogeochemistry, P.O. Box 59, 1790 AB Den Burg, Texel, The Netherlands.
- ⁹Earth & Planetary Sciences Department, University of California, Santa Cruz, CA 95064, USA.
- ¹⁰Department of Earth Sciences, University of Zaragoza, Pedro Cerbuna Street, 12, 50009
- 25 Zaragoza, Spain.
- 26
- 27 Onset of North Atlantic deep water formation is thought to have coincided with Antarctic
- 28 ice sheet growth about 34 million years ago. However, this timing is debated, in part due to
- 29 questions over the geochemical signature of ancient Northern Component Water formed in
- 30 the deep North Atlantic. Here we present detailed geochemical records from North Atlantic
- 31 sediment cores located close to sites of deep water formation. We find that prior to 36
- 32 million years ago, the northwestern Atlantic was stratified, with nutrient-rich, low salinity
- 33 bottom waters. This restricted basin transitioned into a conduit for Northern Component
- 34 Water that began flowing southwards approximately one million years before initial
- 35 Antarctic glaciation. The probable trigger was tectonic adjustments in subarctic seas that
- 36 enabled increased exchange across the Greenland-Scotland Ridge. Increasing surface

salinity and density strengthened Northern Component Water production. The late Eocene
deep water mass differed in its carbon isotopic signature from modern as a result of
leakage of fossil carbon from the Arctic Ocean. Export of this nutrient-laden water
provided a transient pulse of CO₂ to the Earth system perhaps causing short-term
warming, whereas the long-term effect of enhanced NCW formation was greater
northward heat transport that cooled Antarctica.

43

Production of deep water in the North Atlantic Ocean plays a vital role in maintaining the global 44 meridional overturning circulation (MOC)¹. North Atlantic Deep Water (NADW), the lower 45 46 branch of the Atlantic part of the MOC (AMOC), forms in the Labrador and Nordic Seas as 47 surface waters cool and densify. The sinking is largely controlled by an interplay of (i) the 48 stratification at convection sites, determined by the balance of warm salty water from low 49 latitudes, cold freshwater from the Arctic Ocean, and local heat and freshwater fluxes, and (ii) wind-driven upwelling in the Southern Ocean, which returns deep water to the surface^{2,3}. Both 50 51 factors likely impacted the early Cenozoic MOC state, when Atlantic bathymetry and ocean gateways were different and global temperatures were warmer than today^{4,5}. However, resolving 52 their interplay at the onset of NADW production, referred to here as its palaeo pre-cursor 53 54 Northern Component Water (NCW), is challenging because the early history of the AMOC 55 remains poorly constrained.

56

57 Benthic foraminifera δ¹⁸O and δ¹³C records constrain development of global deep water
58 circulation by giving insights into subsurface temperatures, salinity and nutrients⁵. A widely held
59 view is that NCW began filling the Atlantic close to the Eocene-Oligocene greenhouse to

60	icehouse climate transition (EOT), ~34 million years ago (Ma) ^{4,6-9} , or earlier ¹⁰⁻¹³ . Others argue
61	that emergence of significant NCW was delayed until the late Miocene ¹⁴ . Modeling studies
62	diverge, suggesting either no NCW ¹⁵ during the EOT, strengthening/onset of bipolar deep water
63	formation triggered by Drake Passage deepening ¹⁶⁻¹⁸ , or an ocean state with robust NCW
64	throughout ¹⁹ . Previous data studies that argue for a late Eocene onset of NCW production
65	assume that early Cenozoic NCW was nutrient-poor with a high ('young') benthic $\delta^{13}C$ signature
66	similar to modern well ventilated NADW ^{4,10,13,20} . Yet palaeo data from northerly regions suitable
67	for characterizing NCW are lacking.

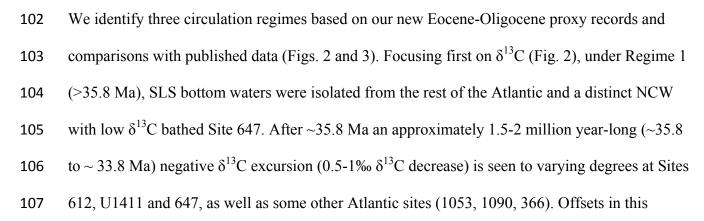
To fill this gap, we produced EOT benthic δ^{13} C and δ^{18} O records from four deep sea sites (>1000 69 70 m palaeodepth) in the high latitude North Atlantic (see Methods and Supplementary Information). Of these, Site 647 in the Southern Labrador Sea (SLS; 47°N, 34 Ma palaeolatitude, 71 72 \sim 2000-3000 m palaeodepth), is the most northerly EOT sequence containing calcareous microfossils necessary for δ^{18} O and δ^{13} C analysis²¹. Additional data for portions of the late 73 74 Eocene were generated from DSDP Sites 112 and 612, and IODP Site U1411 (Fig. 1). The latter 75 two sites should record NCW export in the deep western boundary current (DWBC) (Fig. 1). The data are compared against an Atlantic isotope compilation incorporating 14 previously 76 77 investigated sites (Fig. 2). Records of benthic foraminifera Mg/Ca, fish tooth ENd, and planktic for a for a site δ^{18} O and δ^{13} C from Site 647 and U1411 were also generated to provide constraints 78 79 on bottom water temperature (BWT) and provenance, and water column structure (Methods). 80 The results add unique perspectives on Atlantic end-member deep water properties and changes in circulation during the EOT. 81

82

83 High nutrient content of late Eocene Southern Labrador Sea deep waters

At Site 647 we recognize the typical pattern of δ^{18} O and δ^{13} C increase (>1.0‰ and ~0.5 to 1.0‰ 84 respectively) between 34-33.5 Ma diagnostic of early Oligocene Antarctic glaciation, including 85 the peak in δ^{18} O seen at other sites²², here referred to as the Early Oligocene Glacial Maximum 86 (EOGM) (Fig. 2). The first novel observation at Site 647 is that before ~35.8 Ma, δ^{13} C of SLS 87 bottom water is on average 0.5-1 % lower than all southerly sites. This is opposite to the modern 88 AMOC state, where northern deep waters have the highest δ^{13} C due to sinking of well ventilated, 89 nutrient poor surface waters²³. The low δ^{13} C may reflect nutrient accumulation under stratified 90 91 conditions analogous to the modern North Pacific, i.e. the end of the circulation path. This could imply a southern-sourced deep water filled the SLS during the late Eocene. However, Site 647 92 93 fish debris ε Nd, an isotopic tracer for the origin of deep water masses, bear the fingerprint of a 94 northern hemisphere source ($\epsilon Nd = -11.4$ to -9.4) throughout the studied interval (Fig. 3g). Consequently, we instead argue the low benthic δ^{13} C reflects local bottom water sourced from 95 96 surface waters with a high nutrient concentration, within the narrow, restricted North Atlantic 97 basinal deep water circulation. A probable nutrient source is 'fossil' carbon leaking in from the 98 Arctic Ocean and subarctic seas (Greenland and Norwegian Seas), which had high nutrient stocks during the Eocene because of their semi-isolation, heavily vegetated margins²⁴, and high 99 riverine inflow $^{25-27}$. 100

101



108 excursion's timing between sites are likely caused by age model differences. The phase encompassing the onset and peak of the excursion is Regime 2. Importantly, the δ^{13} C excursions 109 are largest (maximum 1‰) at Sites 612 and U1411 sitting in the DWBC (Fig. 1). While noted 110 previously²⁸, the wider significance of this δ^{13} C excursion has not been fully explored. The 111 observation that Sites 612 and U1411, directly down stream of Site 647, gain benthic δ^{13} C 112 113 signals close to the SLS end-member suggests the signal was propagated from the north. Thus it 114 records southward export of Arctic imprinted, nutrient-rich NCW. The increase in Atlantic benthic δ^{13} C towards the end of Regime 2 indicates that either the pulse of NCW ended, or 115 sufficiently ventilated surface water with higher δ^{13} C was imported to convection sites. Regime 116 117 3, described below, represents the phase where a more mature form of NCW existed.

118

119 Northern deep water cooling, salinification and destratification

A second prominent feature is the pattern of SLS benthic δ^{18} O. The majority of pre-Oligocene 120 δ^{18} O data south of Site 647 range between 0.4-1.2‰ (Fig. 2). Strikingly, in the SLS during 121 Regime 1. benthic δ^{18} O is 1-3% lower than the ensemble. The primary controls on benthic δ^{18} O 122 are BWT and the δ^{18} O composition of seawater, the latter reflecting global glacial ice volume 123 and local salinity. Assuming minimal ice before 34 Ma, the relatively low δ^{18} O in SLS benthos 124 125 indicates a considerably warmer or fresher water mass bathing the seafloor compared to southern stations. Benthic δ^{18} O from Sites 647 and 112 increased gradually from 36.0 to 35.4 Ma, then 126 127 again from ~34.6-34.4 Ma, and had converged close to the dominant Atlantic trend by ~34.3 Ma, i.e. coincident with or just lagging the Atlantic-wide δ^{13} C minimum. Diagenetic alteration of Site 128 647 benthic fossils²⁹ is ruled out due to (i) the excellent fossil calcite preservation²¹ 129 (Supplementary Information), and (ii) the similarity of our new planktic δ^{18} O values from Sites 130

131 647 and U1411 (Fig. 3). Moreover, a similar pattern of decreasing benthic δ¹⁸O is seen in a
132 North Sea record³⁰, although at shallower depths (~500m).

133

134 Mg/Ca BWT help deconvolve temperature and salinity influences on δ^{18} O (Methods and

135 Supplementary Information). Across the EOT, Site 647 Mg/Ca data suggest BWT cooling of

136 $\sim 1^{\circ}$ C combined with a $\sim 0.6\%$ increase in $\delta^{18}O_{sw}$, in agreement with previous studies³¹ (Fig. 3a).

137 From this, we estimate gradual bottom water cooling in the SLS of ~3-4°C between 37.5 Ma to

138 35 Ma, which is similar to observed northern high latitude sea surface $coolings^{32}$. Substituting

139 the Mg/Ca BWTs into a δ^{18} O palaeotemperature equation (Methods) yields ice-free δ^{18} O_{sw}

140 estimates of between -3 to -4 ‰ SMOW during this interval. Based on these $\delta^{18}O_{sw}$ constraints,

141 we estimate late Eocene SLS bottom salinities using relevant modern $\delta^{18}O_{sw}$ -sea surface salinity 142 (SSS) relationships³³ (Fig. 3c).

143

Applying a modern SSS- $\delta^{18}O_{sw}$ relationship from eastern Greenland, today a conduit for low 144 145 salinity (32 PSU) Arctic outflow, implies Site 647 bottom water salinity of 30-32 PSU before 36 146 Ma, increasing by 2-3 PSU from 36 to 34 Ma. The salinity change is similar when a Laptev Sea (today fed by large Siberian rivers) $\delta^{18}O_{sw}$ -salinity regression is applied. While SSS- $\delta^{18}O_{sw}$ 147 148 relationships are spatially widely variable, and modern relationships are only loose analogues for 149 the Eocene, our inferred values are compatible with modern temperature-salinity fields. 150 Therefore, we suggest that (i) before 36 Ma SLS bottom waters were relatively fresh, and (ii) 151 SLS bottom salinity increased from Regime 1 to 2. This conclusion does not change even if samples older than 35 Ma are biased to higher Mg (Supplementary Information) since the 152 salinity signal is embedded in the benthic δ^{18} O, which is independent of Mg/Ca. This 153

interpretation is consistent with that for pre-formed nutrients—they are both likely derived from
the Arctic Ocean. Proxies and models agree that the Arctic had a thick freshwater cap during the
Palaeogene as a consequence of a strong hydrological system and high fluvial inputs under
greenhouse forcing, combined with restricted salt input^{26,33-35}. With no Pacific Ocean outlet at
this time, major surface discharge occurred through the Nordic Seas^{34,36}.

159

Site 647 planktic foraminifera δ^{18} O and δ^{13} C add information on the upper water column. δ^{18} O of 160 161 mixed layer (surface) species is 1-2 % lower than deep-dwellers (subthermocline), consistent with a stratified upper ocean and calcification of mixed-layer dwellers high in the water column 162 or during the warmest season (Fig. 3b). During Regime 1, and before 34.5 Ma, δ^{18} O of the deep-163 164 dwelling planktic species is indistinguishable from benthic foraminifera, reflecting influence of 165 relatively fresh deep water at sub-thermocline levels in the SLS. Site 647 planktic data are sparse 166 before 35 Ma due to low foraminiferal abundance and coring gaps. However, after 34.5 Ma, deep-dwelling planktic and benthic δ^{18} O records separate coincident with the appearance of deep 167 168 water with temperature and salinity properties similar to typical Atlantic values. Additionally, a progressive collapse in the planktic – benthic δ^{13} C gradient (Fig. 3d, e) is documented that 169 captures the SLS water column transitioning from being well-stratified with large vertical δ^{13} C 170 differences (1-1.5 ‰) during Regime 1, to a state with a smaller δ^{13} C gradient (0.5‰) 171 comparable to better-mixed modern North Atlantic convection sites²³ by ~34.3 Ma. Both 172 173 observations are consistent with increasing NCW volume. An abrupt shift in Site 647 benthic 174 assemblages at 34.3 Ma from agglutinated species tolerant of carbonate-poor, nutrient-rich environments, to calcareous species suited to stronger current flow³⁷ coincident with other 175 176 changes (Fig. 3f), provides further evidence for increased convection. Circulation Regime 3

begins at 34.3 Ma, when a saltier, denser form of NCW with higher δ^{13} C is exported through the SLS.

179

180 Deep water sources and sinking

Our Site 647 fish debris ENd data behave as a conservative tracer of northern sourced deep water (see 181 Supplementary Information) and can be compared to published ocean references^{38,39} to identify probable 182 183 NCW source regions (Fig. 3g). While we do not reconstruct Nd directly for Regime 1, our sample from 184 39 Ma is similar to the rest of the record, implying no systematic change in ε Nd and thus bottom water provenance as NCW evolved. The comparison suggests that the Southern Ocean, which has the highest 185 end-member ENd signature in our compilation, was not the source of bottom waters at Site 647. 186 187 Moreover we do not find evidence for the prominent EOT shift to high ENd values found in Southern Ocean records⁴⁰. Previous studies have suggested that prior to deepening of the Greenland Scotland 188 Ridge (GSR) NCW was sourced from the Labrador Sea^{10,13}. Modern Labrador Sea deep water, however, 189 has characteristically low ϵ Nd (~ -14), reflecting erosional inputs from the cratonic hinterland⁴¹. In 190 191 contrast. Site 647 Nd is significantly more radiogenic ($\epsilon Nd = -11.4$ to -9.4), and a closer match to the range of values measured in Nordic sea overflows ($\epsilon Nd = \sim -12.0$ to -8.4)^{41,42} and proximal Arctic Ocean 192 basins above 500 m (ϵ Nd = -11.7 to -8.8)⁴³. A Palaeogene presence of Tethys-sourced deep water at Site 193 647 is another possibility, since the Tethyian ϵ Nd signature (ϵ Nd = -10.0 to -9.3 ^{44,45}) is 194 195 indistinguishable from that of North Atlantic water masses. However, palaeogeographic reconstructions suggest that water mass exchange between European Tethys and Nordic Seas was limited during the 196 middle to late Eocene^{25,46} making this unlikely. 197 198

199 The only connections between the Arctic Ocean and Nordic Seas during the Palaeogene were 200 shallow^{27,46,47}. Transfer of freshened, nutrient-rich waters from the Arctic would have occurred via a proto Greenland Current. Similarity between the North Sea (Kysing-4, borehole) and Site 201 647 benthic δ^{18} O, as well as independent evidence for low salinities in the Nordic Seas^{34,48}, is 202 203 consistent with this picture. Transport from the subarctic seas to the Atlantic Ocean was also 204 shallow, and sinking of Arctic imprinted NCW, must have taken place south of the GSR until it 205 subsided. With sufficient cooling in the subarctic seas, the density contrast of brackish Arctic 206 waters with warmer saltier North Atlantic surface waters permitted sinking, resulting in the 207 distinct bottom water recorded at Site 647.

208

209 Importantly, before ~ 36 Ma, Arctic imprinted NCW deep water formation was minimal, 210 implying regular stratification and stagnation in the SLS. This is consistent with the considerable noise in δ^{13} C and δ^{18} O during Regime 1. How this deep water remained isolated in the SLS at 211 212 depths of around 2000 m under Regime 1 remains uncertain. One possibility is that production 213 and export rates of local deep waters in the North Atlantic were high compared to the influx of 214 southern-sourced deep waters, and subsequently increased further as the cooler, saltier NCW 215 started being produced. Alternatively, bathymetric highs associated with the now extinct 216 Labrador Sea spreading ridges and the West Thulean igneous province to the south, may have isolated SLS subsurface waters from the overall Atlantic during the early Palaeogene⁷. In this 217 218 case, cessation of Labrador Sea spreading close to the EOT was likely important, allowing ridges 219 to subside and enabling enhanced deep water export.

220

221	We illustrate the isotopic evidence and sequence of EOT oceanic changes using natural
222	neighbour re-gridding (Methods) of compiled isotopic data to produce south-north Atlantic
223	depth transects during time windows centered on circulation Regimes 1-3 (Fig. 4, see
224	Supplementary Information for data sources, additional transects and maps). Before ~36 Ma
225	(Regime 1), a strong isotopic δ^{18} O and δ^{13} C depletion effects water masses down to ~2000 m
226	above 40°N (Fig. 4a and b), corresponding to small amounts of low salinity, high nutrient Arctic
227	imprinted NCW in the SLS. The rest of the Atlantic is filled with deep waters with more
228	homogenous δ^{18} O sourced from southerly and possibly low latitude regions ^{10,13} . Increasing
229	subarctic δ^{18} O, reflecting progressive salinification and densification of Nordic surface waters, is
230	accompanied by a 0.5 – 1.0 Myr pulse of NCW export during Regime 2 (Figs. 4 c to h). By 33.3-
231	34.3 Ma the 'fresh' SLS deep water signal no longer exists, bottom water $\delta^{13}C$ increased, the
232	acute phase of low δ^{13} C export is over, and a better-ventilated NCW is exported (Regime 3).
233	Importantly, the initial pulse of NCW export under Regime 2 is recorded by decreasing $\delta^{13}C$
234	signals in deep waters down stream of the SLS. The presence of late Eocene NCW in the
235	Atlantic has not been identified in previous δ^{13} C records ^{10,13,20} because NCW was assumed to
236	have high δ^{13} C signature similar to modern NADW.

238 Causes and consequences of Northern Component Water export

Deepening of the GSR in the late Eocene, for which there is geological evidence^{4,34}, would have
increased Nordic overflows, thus strengthening NCW production. Modelling suggests sill
deepening to 50 m would initiate a threshold switch from lagoonal to estuarine circulation,
salinifying the Nordic Seas sufficiently to intensify northern deep water production³⁴. While this
idea is consistent with our findings, the bathymetric history of the GSR is currently too crude to

accurately date such a change. Moreover, we propose that contemporaneous restrictions to the
Arctic-Nordic Sea exchange also played a role. Geological evidence suggests that the Barents
Sea-Arctic passageway shoaled in the latest Eocene^{46,47} and that relative sea-level variations in
the Arctic were decoupled from global trends from the late Eocene to early Miocene⁴⁹. This
palaeogeographic Arctic isolation enhanced salinification in the Nordic Seas as brackish Arctic
outflows were gradually cut off.

250

251 Changes in NCW production had varied and competing effects. Its onset presumably impacted poleward heat transport in both hemispheres^{17,18}. Initial export of nutrient rich Arctic imprinted 252 NCW may have generated a short-lived pulse of CO₂, on the order of 100-200 ppm, which is 253 consistent with proxy compilations showing a temporary reversal in the falling CO₂ trend 254 between ~34 to ~35 Ma⁵⁰. On the other hand, strengthening of NCW production, and enhanced 255 256 northward ocean heat transport, could have played a role in longer-term CO₂ drawdown due to an accompanying increase in rainfall over land and associated CO₂-weathering feedbacks¹⁶. The 257 258 circulation change timing, 1-2 million years prior to Antarctic glaciation, reinforces the idea that 259 onset of NCW played a role in preconditioning the late Eocene Earth system for the greenhouse 260 to icehouse transition.

261

262 Methods

Methods, including statements of data availability and any associated accession codes andreferences, are available in the online version of this paper.

265

266

267

268 References

- Broecker, W. S. Paleocean circulation during the last deglaciation: A bipolar seesaw?
 Paleoceanography 13, 119-121 (1998).
- 271 2 de Boer, A. M., Toggweiler, J. R. & Sigman, D. M. Atlantic dominance of the meridional
 272 overturning circulation. *J. of Phys. Oceanog.* 38, 435-450 (2008).
- Toggweiler, R. & Samuels, B. Effect of Drake Passage on the global thermohaline
 circulation. *Deep Sea Res.*, *Pt. 1* 42, 477-500 (1995).
- Abelson, M. & Erez, J. The onset of modern-like Atlantic meridional overturning
- 276 circulation at the Eocene-Oligocene transition: Evidence, causes, and possible
- implications for global cooling. *Geochem.*, *Geophys.*, *Geosystems* **18**, 2177-2199 (2017).
- 278 5 Cramer, B. S., Toggweiler, J. R. T., Wright, J. D., Katz, M. E. & Miller, G. H. Ocean
- overturning since the Late Cretaceous: Inferences from a new benthic foraminiferal

isotope compilation. *Paleoceanography* **24**, PA4216 (2009).

- 281 6 Davies, R., Cartwright, J., Pike, J. & Line, C. Early Oligocene initiation of North Atlantic
 282 Deep Water formation. *Nature* 410, 917-920 (2001).
- 283 7 Egloff, J. & Johnson, G. L. Morphology and structure of the Southern Labrador Sea.

284 *Canadian J. of Earth Sci.* **12**, 2111-2133 (1975).

- 8 Miller, K. G. & Tucholke, B. E. in *Structure and development of the Greenland-Scotland*
- 286 *Ridge* (eds M.H.P. Bott, J. Thiede, S. Saxov, & M. Talwani) 549-589 (Plenum Press,
- 287 1983).
- 288 9 Via, R. K. & Thomas, D. J. Evolution of Atlantic thermohaline circulation: Early
- 289 Oligocene onset of deep-water production in the North Atlantic. *Geology* **34**, 441-444
- 290 (2006).

291	10	Borrelli, C., Cramer, B. S. & Katz, M. E. Bipolar Atlantic deepwater circulation in the
292		middle-late Eocene: effects of Southern Ocean gateway openings. Paleoceanography 29,
293		308-327 (2014).
294	11	Boyle, P. R. et al. Cenozoic North Atlantic deep circulation history recorded in contourite
295		drifts, offshore Newfoundland, Canada. Marine Geology 385, 185-203 (2017).
296	12	Hohbein, M. W., Sexton, P. F. & Cartwright, J. A. Onset of North Atlantic Deep Water
297		production coincident with inception of the Cenozoic global cooling trend. Geology 40,
298		255-258 (2012).
299	13	Langton, S. J., Rabideaux, N. M., Borrelli, C. & Katz, M. E. Southeastern Atlantic deep-
300		water evolution during the late-middle Eocene to earliest Oligocene (Ocean Drilling
301		Program Site 1263 and Deep Sea Drilling Project Site 366). Geosphere 12, 1032-1047
302		(2016).
303	14	Wright, J. D. & Miller, K. G. Control of North Atlantic Deep Water circulation by the
304		Greenland-Scotland Ridge. Paleoceanography 11, 157-170 (1996).
305	15	Sijp, W. P., England, M. H. & Huber, M. Effect of the deepening of the Tasman Gateway
306		on the global ocean. Paleoceanography 26, PA4207 (2011).
307	16	Elsworth, G., Galbraith, E., Halverson, G. & Yang, S. Enhanced weathering and CO2
308		drawdown caused by latest Eocene strengthening of the Atlantic meridional overturning
309		circulation. Nat. Geosci. 10, 213-216 (2017).
310	17	Tigchelaar, M., von der Heydt, A. S. & Dijkstra, H. A. A new mechanism for the two-
311		step δ^{18} O signal at the Eocene-Oligocene boundary. <i>Clim. Past</i> 7, 235-247 (2010).
312	18	Zhang, Z. et al. Tropical seaways played a more important role than high latitude
313		seaways in Cenozoic cooling. Clim. Past 7, 801-813 (2011).

314	19	Huber, M. & Sloan, L. C. Heat transport, deep waters, and thermal gradients: Coupled
315		simulation of an Eocene greenhouse climate. Geo. Res. Lett. 28, 3481-3484 (2001).
316	20	Pusz, A. E., Thunell, R. C. & Miller, K. G. Deep water temperature, carbonate ion, and
317		ice volume changes across the Eocene-Oligocene climate transition. Paleoceanography
318		26 , PA2205 (2011).
319	21	Firth, J. V., Eldrett, J. S., Harding, I. C., Coxall, H. K. & Wade, B. Integrated
320		biomagnetochronology for the Palaeogene of ODP Hole 647A: Implications for
321		correlating palaeoceanographic events from high to low latitudes. Geol. Soc. Spec. Pub.
322		373 , 29-78 (2013).
323	22	Coxall, H. K. & Wilson, P. A. Early Oligocene glaciation and productivity in the eastern
324		equatorial Pacific; insights into global carbon cycling. Paleoceanography 26, PA2221
325		(2011).
326	23	Kroopnick, P. The distribution of ¹³ C of $\sum CO_2$ in the world oceans. <i>Deep Sea Res.</i> 32 ,
327		57-84 (1985).
328	24	Golovneva, L. B. Early Palaeogene floras of Spitsbergen and North Atlantic floristic
329		exchange. Acta Universitatis Carolinae, Geologica 44, 39-50 (2000).
330	25	Akhmetiev, M. A. & Beniamovski, V. N. Paleogene floral assemblages around
331		epicontinental seas and straits in Northern Central Eurasia: proxies for climatic and
332		paleogeographic evolution. Geologica Acta 7, 297-309 (2009).
333	26	Gleason, J. D. et al. Early to middle Eocene history of the Arctic Ocean from Nd-Sr
334		isotopes in fossil fish debris, Lomonosov Ridge. Paleoceanography. 24, PA2215 (2009).

335	27	O'Regan, A. M., Williams, C. J., Frey, K. E. & Jakobsson, M. A Synthesis of the long-
336		term paleoclimatic evolution of the Arctic. Oceanography, The changing Arctic Ocean,
337		Special Issue on the International Polar Year (2007–2009) 24, 66-80 (2011).
338	28	Pusz, A. E. et al. in Special Paper of the Geol. Soc. of America. 452, 83-95 (2009).
339	29	Arthur, M. A. et al. in Proceedings of the Ocean Drilling Program, Scientific Results
340		Vol. 105 (eds S.P. Srivastava, M.A. Arthur, B. Clement et al.) 111-135 (Ocean Drilling
341		Program, 1989).
342	30	Nielsen, S. B. et al. The evolution of western Scandinavian topography: A review of
343		Neogene uplift versus the ICE (isostasy-climate-erosion) hypothesis. J. Geodynam. 47,
344		72-95 (2009).
345	31	Lear, C. H., Bailey, T. R., Pearson, P. N. P., Coxall, H. K. & Rosenthal, Y. Cooling and
346		ice growth across the Eocene-Oligocene transition. Geology 36, 251-254 (2008).
347	32	Liu, L. et al. Global cooling during the Eocene-Oligocene climate transition. Science 323,
348		1187-1190 (2009).
349	33	Waddell, L. M. & Moore, T. C. Salinity of the Eocene Arctic Ocean from oxygen isotope
350		analysis of fish bone carbonate. Paleoceanography, PA1S12 (2008).
351	34	Stärz, M., Jokat, W., Knorr, G. & Lohmann, G. Threshold in North Atlantic-Arctic Ocean
352		circulation controlled by the subsidence of the Greenland-Scotland Ridge. Nat. Comm. 8,
353		15681, doi:10.1038/ncomms15681 (2017).
354	35	Roberts, C. D., LeGrande, A. N. & Tripati, A. K. Climate sensitivity to Arctic seaway
355		restriction during the early Paleogene. Earth Planet. Sci. Lett. 286, 576-585 (2009).
356	36	Brinkhuis, H. et al. Episodic fresh surface waters in the Eocene Arctic Ocean. Nature
357		441, 606-609 (2006).

358	37	Kaminski, M. & Ortiz, S. The Eocene-Oligocene turnover of deep-water agglutinated
359		foraminifera at ODP Site 647, Southern Labrador Sea (North Atlantic).
360		<i>Micropaleontology</i> 60 , 53-66 (2014).
361	38	Burton, K. W., Ling, H. F. & O'Nions, R. K. Closure of the Central American isthmus
362		and its effect on deep-water formation in the North Atlantic. Nature 386, 382-385 (1997).
363	39	O'Nions, R. K., Frank, M., von Blanckenburg, F. & Ling, H. F. Secular variation of Nd
364		and Pb isotopes in ferromanganese crusts from the Atlantic, Indian and Pacific Oceans.
365		Earth Planet. Lett. 155, 15-28 (1998).
366	40	Scher, H. D. & Martin, E. E. Timing and climatic consequences of the opening of Drake
367		Passage. Science 312, 428-430 (2006).
368	41	Lambelet, M. et al. Neodymium isotopic composition and concentration in the western
369		North Atlantic Ocean: Results from the GEOTRACES GA02 section. Geochem.
370		Cosmochim. Acta 177, 1-29 (2016).
371	42	Lacan, F. & Jeandel, C. Acquisition of the neodymium isotopic composition of the North

- 372 Atlantic Deep Water. *Geochem.*, *Geophys.*, *Geosystems.* **6** (2005).
- 373 43 Porcelli, D. *et al.* The distribution of neodymium isotopes in Arctic Ocean basins.
- 374 *Geochim. Cosmochim. Acta* **73**, 2645-2659 (2009).
- Grandjean, P., Cappetta, H., Michard, A. & Albarede, F. The assessment of REE patterns
 and 143Nd/144Nd Nd ratios in fish remains. *Earth Planet. Sci. Lett.* 84, 181-196 (1987).
- 377 45 Stille, P. & Fischer, H. Secular variation in the isotopic composition of Nd in Tethys
- 378 seawater. *Geochim. Cosmochim. Acta* **54**, 3139-3145 (1990).
- 379 46 Kharin, G. S. & Lukashina, N. P. Paleogeography of the Norwegian-Greenland and
- northwestern European Sea basins in the Paleogene. *Oceanology* **50**, 226-239 (2010).

381	47	Musatov, E. E. & Pogrebitskij, Y. E. Late Mesozoic-Cenozoic evolution of the Barents	
382		Sea and Kara Sea continental margins. Polarforschung 68, 283-290 (2000).	
383	48	Andreasson, F. P., Schmitz, B. & Spiegler, D. in Proceedings of the Ocean Drilling	
384		Program, Scientific Results. Vol. 151 (eds J. Thiede et al.) 583-591 (Ocean Drilling	
385		Program, 1996).	
386	49	Hegewald, A. & Jokat, W. Relative sea level variations in the Chukchi region - Arctic	
387		Ocean - since the late Eocene. Geophys. Res. Lett. 40, 2013 (2013).	
388	50	Anagnostou, E. et al. Changing atmospheric CO ₂ concentration was the primary driver of	
389		early Cenozoic climate. Nature 533, 380-384 (2016).	
390			
391	Corre	sponding Author Correspondence and requests for materials should be addressed to	
392	Helen Coxall (<u>helen.coxall@geo.su.se</u>).		
393			
394	Acknowledgements Samples were provided by the International Ocean Discovery Program		
395	(IODP), which includes the predecessors the Deep Sea Drilling Project and Ocean Drilling		
396	Program. We thank Julia Becker and Megan Spencer for technical assistance with the stable		
397	isotopes and Hedvig Öste and Emelie Axelsson for preparing the core samples. HKC was		
398	supported by a Royal Society Research Fellowship, Swedish Funding agency (VR) no. DNR		
399	2008-2859 and the Bolin Centre for Climate Research, and TF by NERC Grants NE/I006257/1		
400	and NE/L004607/1. KS acknowledges financial support from the Danish Council for		
401	Indepe	ndent Research/Natural Sciences (DFF/FNU; Grant 11-107497).	
402			

403	Author Contributions HKC and JB conceived the project. HKC directed the research,
404	generated the stable isotope data for Sites 112, 647 and U1411, compiled the proxy records and
405	led writing of the paper. AL produced the new Site 612 data and age model. CHL conducted the
406	trace metal analysis. CH produced and interpreted the Nd data with the help of TF. MO produced
407	the palaeogeographic map for Figure 1 and conducted the subsidence modeling. KS helped
408	produce the Site 647 age model. MH helped with the interpretative framework and produced the
409	interpolated Atlantic depth isotopic transects and maps. JZ and AdB helped interpret the data. All
410	authors contributed to writing the manuscript.
411	
412	Additional information
413	Supplementary information is available in the online version of this paper. The data can be
414	obtained from the 'Bolin Centre for Climate Research' database: http://bolin.su.se/data/Coxall-
415	<u>2018</u> . Reprints and permissions information is available online at www.nature.com/reprints.
416	
417	Competing financial interests
418	The authors declare no competing financial interests.
419	
420	Figure captions
421	
422	Figure 1. Site locations of sections included in this study. Stars identify the new data sets
423	presented here. Map annotations: Red line = Mid Ocean Ridge 34 Ma; white line = position of
424	56 Ma isochron; black line = continent-ocean crust boundary. See Methods Section for details of
425	the palaeogeographic framework and inset map. LS = Labrador Sea, NGS = Norwegian

Greenland Sea; T = Tethys Ocean; GSR = Greenland Scotland Ridge. Inset panel shows the path
of major deep (blue) and surface currents today: Denmark Strait Overflow Water (DSOW);
Iceland-Scotland Overflow Water (ISOW); Labrador Sea Water (LSW); North Atlantic Current
(NAC) and the Deep Western Boundary Current (DWBC).

430

Figures 2. New and published Atlantic benthic δ^{18} O and δ^{13} C (*Cibs.* adjusted). The EOT 431 432 (fine dashed horizontal lines) and the EOGM event are identified by the step-increase and maximum in δ^{18} O in the earliest Oligocene respectively. Trend lines represent smoothed curve 433 434 fits that incorporate a geometric weighting. Regimes 1-3, separated by blue long-dash lines, are phases of ocean circulation defined here based on proxy data. Pale agua shading represents 435 436 transition phases. Vertical black arrows identify time windows gridded in Fig. 4. See 437 Supplementary Information for data sources, age modeling and an expanded figure with 438 additional data.

439

440 Figure 3. Sites 647 and U1411 multiproxy data. a) Mg/Ca BWT; paler blue symbols = 441 maximum BWTs due to potential Fe contamination (Supplementary information). b), d): planktic and benthic δ^{18} O and δ^{13} C (black symbols=equatorial Pacific EOT chemostratigraphic 442 reference²², open symbols =U1411). c) Estimated Site 647 bottom salinity based on modern 443 δ^{18} Osw- relationships; (LS) Laptev Sea, (EG) Eastern Greenland. Error envelopes are based on 444 2STD of the Mg/Ca BWT. e) =Site 647 planktic-benthic δ^{13} C difference and modern gradients²³. 445 f) Site 647 agglutinated benthic foraminifera³⁷. g) Site 647 fish tooth Nd and EOT ocean 446 447 signatures, including Artic ranges (error bars = 2σ standard reproducibility). Annotations as in 448 Fig. 2.

450 Figure 4. Depth-latitude compilation of Atlantic benthic δ^{13} C and δ^{18} O during the late

451 Eocene to early Oligocene constructed using natural neighbor interpolation. Data are plotted

- 452 at their 34 Ma positions (dots indicate core palaeopositions). The five time slices illustrate the
- 453 transition through the three circulation regimes identified here (R1, R2 and R3; see Fig. 2). See
- 454 Supplementary information for data sources and a more extensive set of gridded time slices and
- 455 late Eocene maps.

456

457 METHODS

458

459 Palaeogeographic plate reconstructions and modern Atlantic Ocean circulation inset

- 460 Palaeogeographic plate reconstructions used in production of main text Figure 1 were performed
- using G-plates, with coastlines adapted from E-O reconstructions (34 Ma) of Ron Blakey,
- 462 Colorado Plateau Geosystems, Arizona USA. The inset figure showing modern North Atlantic
- 463 surface and deep current paths is based on the schematics of ref- 51 .
- 464

465 Age framework

- 466 Site 647 age control is based on biomagnetostratigraphy²¹, adjusted here using Site 647 δ^{18} O 467 chemostratigraphy (See Supplementary information for further details for Site 647 and the other
- sites). Site 112 ages are estimated from biostratigraphy⁵². Site U1411 ages are based on IODP
- 469 Exp. 342 shipboard magnetostratigraphy⁵³. The Site 612 age model is based on the
- 470 biostratigraphy of ref-⁵⁴. In all cases, datum events are calibrated or rescaled using linear
- 471 interpolation to the chronology of ref-⁵⁵ to permit comparison with the Atlantic benthic isotope
- 472 stack (after refs $-^{5,56,57}$), much of which exists on this common time scale.
- 473

474 Stable isotopes

- 475 Planktic and benthic foraminifera are present throughout the EOT interval of Site 647, 112 and
- 476 U1411, although heavily diluted by terrestrial clay. Planktic and benthic foraminifera are
- somewhat more common at Site 612. Tests are exceptionally well preserved at all sites
- throughout the studied intervals (see Supplementary Information for further details).
- 479
- 480 For a miniferal δ^{18} O and δ^{13} C for Sites 647 and 112, was derived from the benthic for a minifera
- 481 taxa Oridorsalis umbonatus (shallow infaunal) and Cibicidoides spp. (epifaunal), where
- 482 available, both shown to be a reliable deep-sea tracer in previous studies^{22,58} (see Supplementary
- 483 Information). Site U1411 measurements are on *Cibicidoides* spp. and the new Site 612
- 484 measurements on *Hanzawaia ammophila*. Sites 647 and U1411 planktic foraminiferal analyses
- 485 were made on *Turborotalia ampliapertura* and *Catapsydrax unicavus*, representing surface
- 486 mixed layer and thermocline/subthermocline habitats respectively⁵⁹. Site 647 stable isotope
- 487 analysis was performed at Cardiff University using a ThermoFinnigan MAT252 mass

spectrometer equipped with an automated KIEL III carbonate preparation unit. Additional 488 489 samples were run at the National Oceanographic Centre, Southampton University, using a Europa Geo 20–20 mass spectrometer equipped with a CAPS automatic carbonate preparation 490 system. Standard external analytical precision quoted at Cardiff was better than 0.05% for δ^{18} O 491 and 0.03% for δ^{13} C, and $\pm 0.08\%$ for δ^{18} O and δ^{13} C at Southampton. Site 612 analyses were 492 measured at the Department of Geological Sciences, Stockholm University on a ThermoFinnigan 493 494 MAT 252 IRMS coupled with a Finnigan Gasbench II device. Standard external analytical 495 precision, based on replicate analysis of in-house standards calibrated to international standards (NBS19, IAEA-CO-1 and IAEA-CO-8), was better than 0.07‰ for δ^{13} C and 0.15‰ for δ^{18} O. All 496 497 results are reported relative to the VPDB standard. Our Site 647 O. umbonatus data have been adjusted to Cibicidoides values (believed to be close to ambient seawater) by subtracting -0.28‰ 498 for the δ^{18} O following ref-⁶⁰, and by addition of 1.4‰ to the δ^{13} C, following ref-⁶¹ (consistent 499 with a species comparison study in a restricted basin in the western North Pacific which closely 500 matches our few Site 647 *Cibicidoides-Oridorsalis umbontatus* δ^{13} C pairs). The different species 501 are differentiated in Figs. 2 and 3 by dark red (O. umbontatus) and bright red (Cibicidoides spp.) 502 symbols. For Site 612 the following adjustments (after ref-⁶⁰) were used when integrating the 503 new *H. anmophila* data: $(\delta^{18}O_{H. anmophila} - 0.16)/0.62 = \delta^{18}O_{Cibicidoides}$, and $\delta^{13}C_{H. anmophila} + 0.08 = \delta^{13}C_{Cibicidoides}$. The planktic-benthic $\delta^{13}C$ gradient $(\Delta\delta^{13}C)$ was generated by resampling the 504 505 planktic and benthic foraminifera δ^{13} C curves to provide paired samples. Our new δ^{18} O and δ^{13} C 506 are compared with 21 other Atlantic data sets that build on the compilations of refs-^{5,57}. The new 507 508 data produced in this study are presented in Supplementary Data file S1). See Supplementary 509 Table S1 for the full list of sites meta data and sources used in our Atlantic compilation.

510

511 Trace metal analysis and Mg/Ca for a miniferal bottom water palaeothermometry

Trace metal content (Mg/Ca, Mn/Ca, Fe/Ca) was analyzed on Site 647 O. umbonatus. Prior to 512 analysis, benthic foraminifera samples were cleaned following the protocol of refs-^{62,63} leaving 513 out the reducing step due to the scarcity of material but including contaminant removal under 514 binocular microscope following the oxidative step⁶⁴. Samples were subjected to one weak acid 515 516 leach prior to dissolution and dilution. Analysis was carried out at Cardiff University on a 517 Thermo Element XR ICP-MS against standards with equivalent Ca concentration. Multi-element 518 standards were made in-house from single element standards supplied by Greyhound 519 Chromatography and Allied Chemicals. Analytical precisions determined from separate consistency standards over the course of a year are 0.5% for Mg/Ca, and 2% for Mn/Ca and 520 Fe/Ca (rsd). Mg/Ca paleo- bottom water temperatures (BWT) were calculated using the 521 exponential calibration of ref-⁵⁸ (See Supplementary Information and Supplementary Data file 522 S2).

523 524

Our O. umbonatus Mg/Ca record is noisy and high Mg/Ca ratios are often associated with high 525 Fe/Ca (correlation coefficient $r^2 = 0.4$) (Supplementary Data file S2). By excluding the samples 526 with Fe/Ca >> 900 μ mol/mol, r² was reduced to 0.18. The subset of data, with lower Fe/Ca, 527 largely the upper portion of the core in samples younger than 34.5 Ma (Supplementary Table 528 529 S4), may be regarded as most reliable. However, despite the higher Fe/Ca in the older samples, we believe the Mg/Ca data from the lower part of the core are not entirely flawed since the Fe/Ca 530 vs Mg/Ca r^2 value based on the full sample set is still relatively low and there is Mg/Ca overlap 531 of higher and lower Fe/Ca Mg/Ca around the EOT (Main Figure 3A, paler blue symbols). Thus, 532 the older Mg/Ca should provide realistic palaeo-bottom water temperatures (within the 533

- uncertainties of the method), and are thus included in the down core record to provide ballpark
- 535 BWTs and allow salinity reconstructions in the initial part of the late Eocene.
- 536

537 Bottom Water Salinity reconstruction

The pattern of progressive benthic δ^{18} O increase and maximum 4°C BWT cooling between 37.5-35.5 Ma implies that sea water δ^{18} O (δ^{18} O_{sw}) was changing over this period. To explore this

540 further bottom water palaeosalinity was reconstructed based on modern sea surface salinity

541 (SSS) - δ^{18} O relationships. This was performed in two steps. First, δ^{18} O_{sw} values were calculated

by substituting the Site 647 Mg/Ca BWTs into the δ^{18} O-benthic foraminifera palaeotemperature equation of ref-⁶⁵. Due to the noise in our estimated benthic bottom water temperatures we used

broad 'BWT brackets', based on mean BWT values for three intervals (Supplementary Table
545 S5).

546

547 Second, bottom water palaeosalinity was reconstructed based on the modern surface salinity δ^{18} O 548 relationships for the Laptev Sea and East Greenland Current^{66,67}, regions with relatively low

549 $\delta^{18}O_{sw}$ linked to the Arctic Ocean or Arctic outflows respectively (the Laptev Sea is an Arctic

shelf sea that receives large volumes of river run-off from Siberian rivers (22-34 PSU), while the

551 East Greenland Current carries low salinity surface waters (32 PSU) out of the Arctic Ocean). It

52 was assumed that these relationships remained the same down core.

553

554	Laptev Sea:	Salinity= $(\delta^{18}O_{sw} - 18.86) = 0.5$	$R^2 = 0.98 \text{ ref-}^{66}$
555	East Greenland:	Salinity= $(\delta^{18}O_{sw} - 35.02) = 1.01$	ref- ⁶⁷

556

557 The resulting curve, which is plotted as a 'smoothed curve-fit' in KaleidaGraph® with error 558 envelopes representing limits determined by 2σ of the BWT brackets (Main Fig. 3C), provides 559 coarse constraints on the evolution of Site 647 bottom water salinity in the late Eocene. As 560 discussed above, its possible that the decreasing Mg/Ca between 37.5-35.5 Ma represents 561 decreasing trace metal contamination rather than BW cooling. If this is the case then the BWTs around 37 Ma are too high, which would bias the salinities to too salty values. Thus, including or 562 excluding the older Mg/Ca data does not change the conclusions. We have confidence in the 563 Mg/Ca after 34 Ma and thus have δ^{18} Osw constrained there. The important point is that the 564 subsurface densification signal is seen in the benthic foraminifera δ^{18} O record (increasing δ^{18} O 565 566 from 37.5-35.5 Ma). It is impossible that this is an artifact of the Mg/Ca data.

567568 Neodymium isotope methodology

569 Fish teeth and bone debris were hand-picked from the >63µm fraction of sieved sediment and 570 cleaned to remove adhering debris. Initial experiments (see Supplementary information) indicated that a the 'simple cleaning method' of ref-⁶⁸ was sufficient. All samples were dissolved 571 572 in 2M HCl, dried and converted to nitrate form prior to column chemistry. A standard two-stage 573 ion chromatography procedure was used, which first isolated the REEs from the sample matrix 574 using TRU Spec resin (100-120µm bead size) and then separated Nd from the other REE's with Ln-Spec resin (50-100µm bead size) (after ref-⁶⁹). Neodymium isotope ratios were measured on 575 a Nu Plasma MC-ICP-MS at Imperial College London in static mode. Instrumental mass bias 576 was corrected for using a 146 Nd/ 144 Nd ratio of 0.7219. Samarium interference can be adequately 577 corrected if the ¹⁴⁴Sm signal contributes less than 0.1% of the ¹⁴⁴Nd signal. The Sm contribution 578 579 in all our samples was well below this level. Chemistry blanks were consistently below 10pg

- Nd. Replicate analyses of the Nd standard JNdi vielded 143 Nd/ 144 Nd ratios from 0.512060 ± 580 0.000015 to 0.512251 ± 0.000015 (n=116), dependent on daily running conditions over 12 581 582 months. The external reproducibility of our chemistry and mass spectrometry procedure was 583 monitored using a fossil bone composite standard supplied by Clive Trueman (University of Southampton) yielding a ¹⁴³Nd/¹⁴⁴Nd ratio of 0.512377 ± 0.000028 (n=8 over 18 months), which agrees within error with previously published values^{70,71}. We note that the standard material was 584 585 digested for analysis following the methods in ref⁷⁰ for analytical consistency. Briefly, 50 mg of 586 material was digested in 3M HNO₃ in a Teflon beaker at 130°C. Any material remaining after 587 this step was subjected to a further 48 hours digestion in a 3:1 mixture of 15M HNO₃ to 27M HF. 588 To correct for the decay of 147 Sm to 143 Nd within the fish teeth over time we use rare earth 589 element concentrations obtained in two samples from this site. Derived ¹⁴⁷Sm/¹⁴³Nd ratios of 590 0.129 and 0.134 are consistent with values reported in other studies⁷²⁻⁷⁴. We applied an average 591 value of our measurements (147 Sm/ 143 Nd = 0.132) to all remaining samples. All Nd isotope ratios 592 593 are reported in epsilon notation (ε_{Nd}) (Supplementary Table 6). Comparative ε_{Nd} data in Figure 3 are listed in Supplementary Table S7. 594
- 595

596 Atlantic isotopic depth sections

- 597 We used standard techniques in ocean data assimilation to create homogenized and interpolated
- 598 maps of isotopic values based on the sparse data (see Supplementary Table S1 for site
- information, data sources and a more complete set of maps; SI Figs 9A-L). For the transects the
- 600 proxy data were placed on to a regular latitude-depth grid based on their reconstructed depths
- and palaeo-locations, and the natural neighbor regridding routines implemented in the NCAR
 Command Language were used to create interpolated, gridded values
- 603 (https://www.ncl.ucar.edu/Document/Functions/Built-in/natgrid.shtml). Extrapolation beyond the
- 604 convex hull of the kernel was not used. The background palaeogeography is based on Ref-⁷⁵
- 605 (hotspot reference frame). The differences in interpretation for our paper using the alternative
- 606 Palaeomag reference frame described in the same study are negligible.
- 607
- For the maps, the proxy records interpolated using the technique of Barnes-Cressman iteratedobjective analysis implemented in the NCAR Command Language
- 610 (www.ncl.ucar.edu/Document/ Functions/Contributed/obj anal ic Wrap.shtml). In this
- 611 approach, each observation is assigned a circular radius of influence, R. Here, we used
- 612 successive values of R of 9° , 8° , 6° , 4° , 2° , 1° . A first guess of the value at every grid point was
- 613 made by including all observations within the region of influence of that grid point. A distance-
- 614 weighted average of the differences between the first-guess fields and the actual observations
- 615 was made, and this anomaly was added into the first-guess fields to calculate a second-guess
- 616 field. Thus, observations from beyond the radius of influence were ignored in updating the field,
- and other observations closer to the initial observation were given greater weight. This was done
- 618 for all grid points under consideration. The resulting fields were used as the basis for the next
- 619 iteration, which was carried out with a smaller region of influence.
- 620

621 Data availability statement

- 622 The authors declare that lists of the sources of previously published data used in this study are
- 623 available within the article and its Supplementary Information files. The new data are available
- at the Bolin Centre for Climate Research Database: <u>http://bolin.su.se/data/Coxall-2018</u>.
- 625

626	References		
627			
628			
629	51	Schmitz, W. J. & McCartney, M. S. On the North Atlantic Circulation. Rev. of Geophys.	
630		31, 29-49 (1993).	
631	52	Laughton, A. S. et al. Site 112, in Initial Reports of the Deep Sea Drilling Project, Vol.	
632		12 (eds A.S. Laughton, W. A. Berggren et al.) 161-253 (US Goverment Printing Office,	
633		1972).	
634	53	Norris, R. D., Wilson, P. A., Blum, P. & the Expedition Scientists, Proceedings of the	
635 636		<i>Integrated Ocean Drilling Program</i> , 342 , doi:10.2204/iodp.proc.342.2014 (Integrated Ocean Drilling Program, 2014).	
	51		
637	54	Miller, K. G. & Katz, M. E. in <i>Initial Reports of the Deep Sea Drilling Project</i> , Vol. 95	
638		(eds C. W. Poag, A. B. Watts <i>et al.</i>) 267-298 (U.S. Government Printing Office, 1987).	
639	55	Cande, S. C. & Kent, D. V. Revised calibration of the geomagnetic polarity timescale for	
640	• 6	the Late Cretaceous and Cenozoic. J. Geophys. Res. 100, 6093-6095 (1995).	
641	56	Zachos, J. C., Pagani, M., Sloan, L. C., Thomas, E. & Billups, K. Trends, rhythms, and	
642		aberrations in global climate 65 Ma to present. Science 292, 686-693 (2001).	
643	57	Zachos, J. C., Dickens, G. R. & Zeebe, R. E. An early Cenozoic perspective on	
644		greenhouse warming and carbon-cycle dynamics. Nature 451, 279-283 (2008).	
645	58	Lear, C. H. et al. Neogene ice volume and ocean temperatures: Insights from infaunal	
646		foraminiferal Mg/Ca paleothermometry. Paleoceanography 30, 1437-1454 (2015).	
647	59	Pearson, P. N. et al. Warm tropical sea surface temperatures in the Late Cretaceous and	
648		Eocene epochs. <i>Nature</i> 413 , 481-487 (2001).	
649	60	Katz, M. E. et al. Early Cenozoic benthic foraminiferal isotopes: species reliability and	
650		interspecies correction factors. Paleoceanography 18, 1024 (2003).	
651	61	Rathburn, A. E., Corliss, B. H., Tappa, K. D. & Lohmann, K. C. Comparisons of the	
652		ecology and stable isotopic compositions of living (stained) benthic foraminifera from the	
653		Sulu and South China Seas. Deep Sea Res. Pt 1. Oceanographic research papers 43,	
654		1617-1646 (1996).	
655	62	Boyle, E. A. Manganese carbonate overgrowths on foraminifera tests. Geochim.	
656		Cosmochim. Acta 47, 1815-1819 (1983).	
657	63	Boyle, E. A. & Keigwin, L. D. Comparison of Atlantic and Pacific paleochemical records	
658		for the last 215,000 years: changes in deep ocean circulation and chemical inventories.	
659		Earth Planet. Sci. Lett. 76, 135-150 (1985).	
660	64	Barker, S., Greaves, M. & Elderfield, H. A study of cleaning procedures used for	
661		foraminiferal Mg/Ca paleothermometry. Geochem., Geophys., Geosystems 4,	
662		doi:10.1029/2003GC000559 (2003).	
663	65	Marchitto, T. M. et al. Improved oxygen isotope temperature calibrations for	
664		cosmopolitan benthic foraminifera. Geochim. Cosmochim. Acta 130, 1-11 (2014).	
665	66	Mueller-Lupp, T., Erlenkueser, H. & Bauch, H. A. Seasonal and interannual variability of	
666		Siberian river discharge in the Laptev Sea inferred from stable isotopes in modern	
667		bivalves. Boreas 32 , 292-303 (2003).	
668	67	Fairbanks, R. G., Charles, C. D. & Wright, J. D. in Radiocarbon After Four Decades (ed	
669		R. E. Taylor) 473-500 (Springer, 1992).	
670	68	Martin, E. E. & Haley, B. A. Fossil fish teeth as proxies for seawater Sr and Nd isotopes.	
671		Geochim. Cosmochim. Acta 64, 835-847 (2000).	

- 69 Pin, C. & Zalduegui, J. S. Sequential separation of light rare-earth elements, thorium and
 673 uranium by miniaturized extraction chromatography: application to isotopic analyses of
 674 silicate rocks. *Analyt. Chimica Acta* 339, 79-89 (1997).
- 675 70 Chavagnac, V. *et al.* Towards the development of a fossil bone geochemical standard: An
 676 inter-laboratory study. *Analyt. Chimica Acta* 599, 177-190 (2007).
- Scher, H. D. & Delaney, M. L. Breaking the glass ceiling for high resolution Nd isotope
 records in early Cenozoic paleoceanography. *Chem. Geol.* 269, 329-338 (2010).
- Thomas, D. J., Bralower, T. J. & Jones, C. E. Neodymium isotopic reconstruction of late
 Paleocene-early Eocene thermohaline circulation. *Earth Planet. Sci. Lett.* 209, 309-322
 (2003).
- 682 73 Martin, E. E. & Scher, H. A Nd isotopic study of southern sourced waters and Indonesian
 683 throughflow at intermediate depths in the Cenozoic Indian Ocean. *Geochem. Geophys.*684 *Geosystems* 7, Q09N02 (2006).
- Moiroud, M. *et al.* Evolution of the neodymium isotopic signature of neritic seawater on
 a northwestern Pacific margin: new constrains on possible end-members for the
 composition of deep-water masses in the Late Cretaceous ocean. *Chem. Geol.* 356, 160170 (2013).
- Baatsen, M. *et al.* A generalised approach to reconstructing geographical boundary conditions for palaeoclimate modelling. *Clim. Past.* 12, 4917-4942 (2016).
- 691

